

*Article*

## The Effect of Water Evaporation in Automotive Windshield Defrosting

Phanatorn Amnuayphan, Rattapon Thanapatpanich, Prabhath De Silva\*,  
and Pinunta Rojratsirikul

International School of Engineering, Faculty of Engineering, Chulalongkorn University, Bangkok  
10330, Thailand

\*E-mail: prabhath.d@chula.ac.th (Corresponding author)

**Abstract.** Water evaporation during windshield defrosting is investigated paying particular attention to the effects of air humidity and wind speed. During the defrosting process, the ice layer on the windshield begins to melt as the temperature of the defrost air increases. Results have shown that the ice-turned-water can evaporate depending upon the ambient air humidity level and the wind speed. Water evaporation takes the heat otherwise available for melting, thereby delaying the ice melting process. It is found that at low wind speeds the effect of air humidity in delaying the ice-melting is minimal. However, at high wind speeds, ( $>10$  m/s) water evaporation can take enough heat away from melting, thereby significantly reducing the ice removal rate. In relation to this, driver safety concerns associated with the reduction of ice melting rate are discussed.

**Keywords:** Windshield defrosting, water re-freeze, automotive vision safety.

ENGINEERING JOURNAL Volume 23 Issue 4

Received 5 February 2019

Accepted 16 May 2019

Published 8 August 2019

Online at <http://www.engj.org/>

DOI:10.4186/ej.2019.23.4.107

## 1. Introduction

Unobstructed visibility through the windshield and window glasses of an automobile is of paramount importance for driver and occupant safety. While dust and debris may also hinder visibility, frost or ice formation on the exterior glass surfaces is a particular concern to drivers in cold climates. Frost or ice build-up during winter can significantly reduce the driver's visibility. Once ice is formed and has adhered to the windshield glass, wipers may slide-over and offer little help in removing ice. While manual cleaning of ice is not possible when the vehicle is in motion, use of windshield wipers may help reduce further build-up. Wipers are not available for front side windows, which need to be free from frost for clear visibility to the side window mirrors. As such, government mandated safety requirements dictate that automotive manufacturers design the Heating, Ventilating and Air Conditioning (HVAC) system such that hot defrost air should be able to clear ice formed on the windshield and also prevent further build-up. The HVAC system blows warm air over the inside surface of the windshield glass and allows heat conduction across the glass to melt ice formed on the windshield exterior surface. Compliance to the mandated requirements dictates that a certain percentage of windshield area is cleared from ice at chosen times [1].

### 1.1. Windshield Defrost Testing and Validation

In preparation for a typical windshield defrosting test, an ice-layer is applied on the windshield of the vehicle that is pre-soaked in a climatic wind tunnel at a temperature below the freezing point of water. The ice melting pattern is then traced at regular time intervals as the warm defrost air gradually clears the ice layer. Some drawbacks of conducting climatic wind tunnel tests are that they are costly and that they demand careful planning and preparation. As such, computational fluid dynamics (CFD) simulations offering both qualitative and quantitative analysis have become abundant in recent years. It is common to use CFD simulations to optimize defrost duct/grille shapes, to estimate cabin interior air flow rates [2–4], and also to quantify ice melting rates in subsequent vehicle development [5, 6]. CFD models simulate and predict the melting pattern and the rate of removal of the ice-layer that is applied on the glass exterior surfaces. The results are often presented as the time evolution of contours of liquid fraction of ice/water mixture. The liquid fraction  $\gamma$  is defined as,

$$\gamma = \begin{cases} 0, & T < T_s \\ \frac{T-T_s}{T_l-T_s}, & T_l < T < T_s \\ 1, & T > T_l \end{cases} \quad (1)$$

where,  $T$  is the temperature of the ice-water mixture,  $T_s$  is the solidus temperature and  $T_l$  is the liquidus temperature.

CFD analysis as a tool in optimizing defrost duct and grille shapes has been adequately shown. Such efforts significantly cut down the number of design and development iterations, hence helping to reduce cost by eliminating tooling, prototyping, and wind tunnel testing. The advantages of incorporating HVAC system in vehicle level simulations [3, 4] have been outlined and good agreement of simulation results with experimental data have been reported [6, 7]. Simulation studies are able to identify design problem areas, hence faster and more economical ways to circumvent them become easier [8].

The performance of HVAC system in the vehicle cabin environment has continued to gain interest during the last decade. Park et al. [9] simulated the flow and temperature field on the interior of a cabin when the hot air was discharged from the defrost nozzle. Kader et al. [10] used both numerical and experimental methods to study the airflow, temperature distribution, humidity and frost melting pattern near a vehicle windshield and inside the compartment. The defrosting performance was found to be more efficient when the injection angle of the nozzle was between 15 to 25 degrees. CFD analysis can successfully be used to locate dead zones due to nonuniform temperature on the windshield [10–12]. CFD analysis still continues to support the industry as a development tool in enhancing defrosting performance [13] ensuring that the legal defrosting/defogging requirements are satisfied [14]. Its application in novel additions such as in electric EV vehicles [15], has been reported as well.

## 1.2. Water Pool Evaporation

Evaporation from exposed water surfaces is a common occurrence in nature. The rate of evaporation depends on the surrounding air temperature, the air humidity level and the water surface temperature. In the absence of wind, air adjacent to water becomes saturated, hence lighter than the surrounding air. As a consequence, this lighter air rises due to natural convection. Air velocity has a significant influence on the evaporation rate as the forced air moves the saturated air just above the interface away. There are practical needs in estimating water evaporation in indoor pools as such estimates dictate the sizing of air conditioning equipment. Although kinetic theory can be used to describe the mass transfer across the air-water interface, empirical correlations [16–20] are commonly used to quantify the amount of evaporation.

A well known and often used equation quantifying the water evaporation in indoor pools is given in ASHRAE [21].

$$m_e = (0.089 + 0.0782V)(p_w - \phi p_a)/h_{fg} \quad (2)$$

where  $m_e$  is the water evaporation rate,  $V$  is the wind speed,  $\phi$  is the relative humidity of the air,  $p_w$  is the saturated vapor pressure at water surface temperature ( $T_w$ ),  $p_a$  is the saturated vapor pressure at air temperature, and  $h_{fg}$  is the latent heat of vaporization. Equation (2) has been particularly used in ventilating and air-conditioning applications. Slightly different formula has been proposed by Shah [18]. Detailed accounts on limitations and its use can be found in [18, 19, 22, 23]. Shah [19] also outlined how to extend the formulas to small-scale situations such as water spills etc. Novel methods employing neural networks [20], and recent CFD based analysis [24] modeling humid air at the air-water interface have also been proposed. Results of Blazquez et al. [24] have shown good agreement with experimental data. However, such an analysis cannot be used in conjunction with the CFD simulation procedure adopted in the present paper.

Work of Smith et al [25] showed that about 56% of the energy load is spent due to water evaporation from outdoor swimming pools when the surrounding air humidity was between (27-65)% and wind speeds were up to 2.2 m/s. Their results, as well as other laboratory testing [23], indicated slightly lower evaporation rates than that predicted by ASHRAE. Work of Jodat et al. [26] consisted of experiments in which the wind velocities were in the range (0.05 – 5) m/s.

Figure 1 illustrates Eq. (2) graphically. It offers a clear visual presentation of the three parameters involved; the air humidity, the water surface temperature and the wind speed. The air temperature is taken as  $-4^\circ\text{C}$ . As Fig. 1 depicts, dry air alone does not result in an enhanced rate of evaporation. The wind speed and the temperature of the water surface have significant effects amplifying the dryness of the air in enhancing the evaporation. Work of Raimundo et al. [27] and Blazquez et al. [24] have shown similar conclusions based on their experimental and numerical studies.

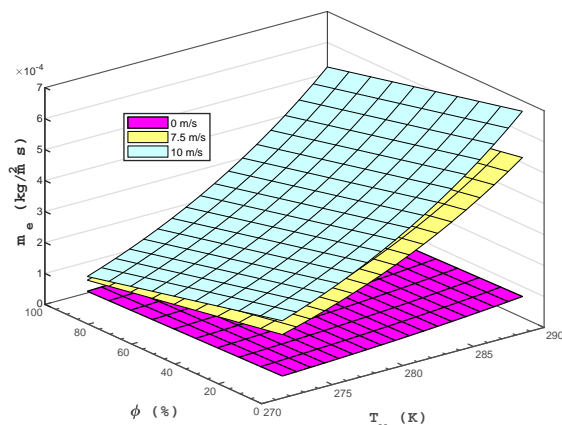


Fig. 1. Dependence of water evaporation rate on air humidity, water surface temperature and wind speed. The air temperature is  $-4^\circ\text{C}$ .

### 1.3. Effect of Evaporation on Windshield Defrosting

Water evaporation can have an influence on the windshield defrosting process. Depending upon the air humidity level and the wind speed, ice-turned-water can take heat away by evaporation, a process that is detrimental to defrosting as heat energy is best utilized for melting rather than for evaporation. The latent heat of vaporization of water (2450 kJ/kg) is approximately seven times larger than that of melting (334 kJ/kg). Hence, even a small amount of water evaporation can have a significant effect.

Climatic wind tunnel defrosting tests often show that initial breakthrough of the ice layer occurs above the region where the defrost air impinges on windshield. Melting initiates from this region and gradually spreads outward along the windshield as time progresses. Thus, a pool of water that is surrounded by ice comes into existence as depicted schematically in Fig. 2.

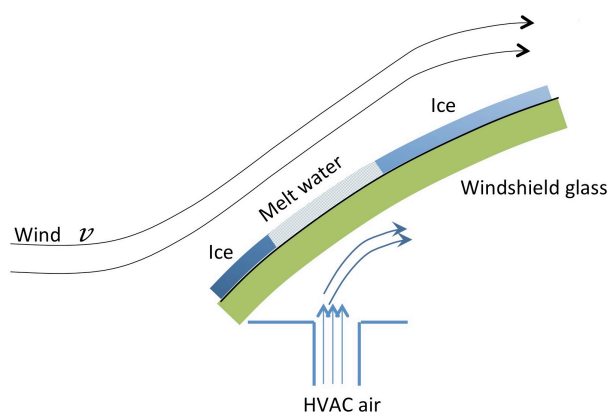


Fig. 2. Schematic of the ice-melting in windshield defrosting. Melt water first appears just above the region where the defrost air impinges.

In the absence of wind in an outdoor environment or the absence of mean air velocity in a climatic wind tunnel, air just above the ice-turned-water pool may become closer to saturation. Thus, water evaporation and subsequent propagation is mainly due to the diffusion of water vapor. In the presence of wind, evaporated moisture is readily taken away by advection, hence the rate of evaporation is much higher. This effect can also be seen in Eq. (2). The latent heat required for evaporation is taken from the water just beneath the top surface. The heat conducted away from neighboring areas causes a delay in ice-melting in those areas. If these conditions exist, it is also possible that some already melted water may refreeze.

The CFD simulation studies relating windshield defrosting mentioned earlier have been carried out mostly to complement wind tunnel testing. Some studies also served the purpose of improving simulation techniques and methodologies. To the authors' knowledge, in all studies, the possibility of water evaporation and its adverse effect have not been considered. In this paper, how water evaporation affects the defrosting process is investigated using CFD simulations.

## 2. Methodology

The approach adopted in this study is to perform windshield defrosting simulations using CFD. The ambient air temperature and the initial temperature of the flow domain is set at  $-4^{\circ}\text{C}$ . During testing, the defrost air is gradually warmed up by the engine heat, and as a result the ice-layer on windshield begins to melt. The defrost air mass flow rate was kept constant at 0.03 kg/s and the defrost air warm up profile was the same for all runs in the study. Four different relative humidity values 20%, 30%, 40%, 100% and three different wind speeds 0 m/s, 7.5 m/s, 10 m/s, were considered.

The material properties used are given in Table 1. Figure 3 shows the vehicle model used for the simulations. It consists of the defrost duct and a schematic representation of the vehicle cabin interior. The overall dimensions of the model are 2.81 m  $\times$  0.68 m  $\times$  1.23 m. Only half of the cabin is considered

Table 1. Material properties used in the simulation.

Material	Density (kg/m <sup>3</sup> )	Heat Capacity (J/kgK)	Thermal Conductivity (W/mK)
Air	1.015	1006	0.0242
Ice	915	2108	2.2
Glass	2500	800	0.8

with the intention of invoking a symmetry condition about the longitudinal mid-plane of the vehicle. Ambient air enters the cabin through the duct inlet and leaves at the back of the cabin.

The vehicle model envelope surface was meshed with triangular elements, and the cabin interior volume was meshed with tetrahedral cells. Windshield glass is represented as a solid by creating prism layers on triangular surface elements. Similarly, a thin ice-layer is represented by generating prism layers on the glass outside surface of the windshield. The total cell count of the model is approximately 1.97 million.

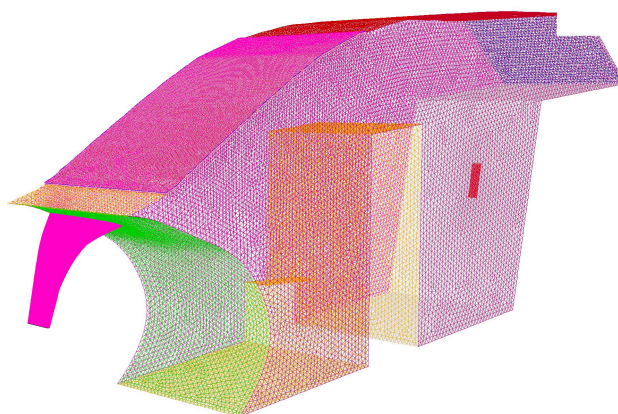


Fig. 3. The full-scale vehicle cabin model used in the study. Only half of the vehicle is used employing mid-plane symmetry boundary condition.

An external C-code (User Defined Function, UDF) that calculates the water evaporation using Eq. (2) was used. It incorporates the ambient air temperature, the relative humidity, and the wind speed as input parameters. The saturation vapor pressure (in *mbar*) is calculated as a function of the temperature using the formula [28],

$$p_a = a_1 + \sum_{n=2}^7 a_n (T_a - T_{ref})^{n-1} \quad (3)$$

where  $T_a$  is the absolute temperature of the air and ( $T_{ref} = 273.15$  K) is a reference temperature. The coefficients  $a_1$  to  $a_n$  in Eq. (3) are given in Table 2.

The CFD simulations were accomplished using ANSYS software package. Only half of the cabin is used as the computational domain by invoking symmetry boundary condition about the vertical longitudinal mid-plane of the vehicle. In order to minimize the computational time, the model is first run isothermally at the ambient air temperature with only momentum and turbulence equations. Once the flow solution is converged, the energy equation is run using the converged frozen flow field. The turbulence field is modeled using standard  $k - \epsilon$  equations. The residuals for the convergence of the flow field are set at  $10^{-5}$ . In transient simulations the temperature field and the liquid fraction of the

Table 2. Coefficients and their values in Eq. (3).

Coefficient	Value
$a_1$	$0.611176750 \times 10^1$
$a_2$	$0.443986062 \times 10^0$
$a_3$	$0.143053301 \times 10^{-1}$
$a_4$	$0.265027242 \times 10^{-3}$
$a_5$	$0.302246994 \times 10^{-5}$
$a_6$	$0.203886313 \times 10^{-7}$
$a_7$	$0.638780966 \times 10^{-10}$

ice-water layer are sought at each time step. A constant time step of 1 s is used throughout for a total simulation period of 2400 s.

In order to simplify the simulations, all surfaces of the vehicle envelope except the ice-layer are assumed to be adiabatic. Thus, the initial heat loss to the ambient is primarily due to convection from the solid-ice layer. The conjugate heat transfer between solid-ice layer and air can be computed numerically [29,30], or using empirical formulae. In still air, this heat loss from the top of the ice-layer to the ambient is from natural convection. The convective heat transfer coefficient  $h$  of the ice-layer exterior surface may be estimated using the well known formula [31] for the natural convection on an inclined surface,

$$h = \frac{k}{L} \left\{ 0.825 + \frac{0.387Ra^{1/6}}{[1 + (0.492/Pr)^{9/16}]^{8/27}} \right\}^2 \quad (4)$$

where  $L$  is the slant height of the windshield, and  $k, \nu, \alpha$ , and  $Pr = \nu/\alpha$  are the thermal conductivity, the kinematic viscosity, the thermal diffusivity, and the Prandtl number of the ambient air, respectively. The Rayleigh number,  $Ra$ , is defined as,

$$Ra = \frac{g'\beta(T_o - T_a)L^3}{\nu\alpha} \quad (5)$$

where  $g' = g\cos(\theta)$ , and  $g$  is the acceleration due to gravity,  $\theta$  is the windshield angle to the vertical,  $\beta$  is the coefficient of thermal expansion, and  $T_o$  is the temperature of the exterior surface of the ice layer.

For the range of wind speeds considered in the study, the maximum Reynolds number was,  $Re = 8 \times 10^5$ , at the highest wind speed of 10 m/s indicating that the boundary layer remains laminar for the most of the windshield. Thus, in the presence of wind, the heat transfer from ice to the ambient air may be assumed to be due to laminar forced convection and the average heat transfer may be estimated as,

$$h = 0.664 \frac{k}{L} Re^{1/2} Pr^{1/3} \quad (6)$$

where  $Re = VL/\nu$ , is the Reynolds number.

Once liquid water appears on the windshield, the UDF calculates the amount of water evaporation based on Eq. (2) at each time step. The resulting latent heat taken away by air is applied as a heat loss to the outside surface of ice-turned-water regions. On the regions of the windshield, where ice is still present, convective heat transfer coefficient is invoked as the thermal boundary condition. It is calculated using Eq. (4) in still air, and using Eq. (6) under forced wind.

The simulations ensure that the cumulative sum of water that can evaporate from any surface element of the ice-water layer is less than the amount of ice initially applied. Thus, for each surface element of the ice-water layer, evaporation is not allowed when the condition given in Eq. (7) is violated.

$$\int_0^t m_e dt < \rho \Delta x \quad (7)$$

Here,  $\Delta x$  is the initial thickness of the ice layer and  $\rho$  is the density of ice.

### 3. Results

Figure 4 shows the pathlines emanating from the duct inlet passing through the defrost duct itself and the vehicle cabin. The pathlines also confirm the symmetry boundary condition about the vertical mid plane of the flow domain. As can be expected, the air velocity is much higher within the duct section compared to that inside the cabin interior. Figure 5 shows the contours of the surface temperature and

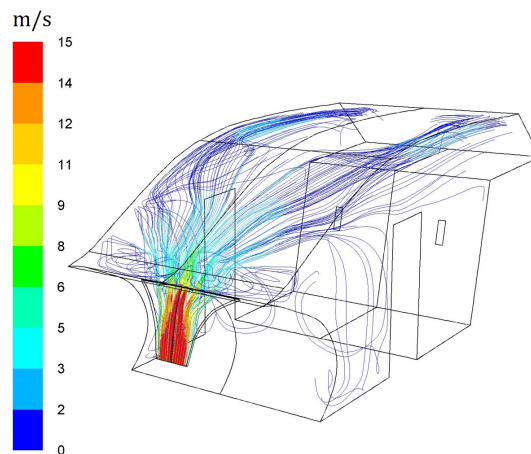


Fig. 4. Airflow pathlines, colored by velocity magnitude, emanating from the duct inlet.

the surface heat flux of the ice-water exterior surface at time  $t = 2400$  s for a simulation with wind speed of 10 m/s and relative humidity of 30%. The surface temperature is a maximum in the vicinity of the area just above the region where warm air directed from the defrost duct as seen in Fig. 5(a). Away from this region, the surface temperature of the ice/water mixture remains near ambient. This observation is in agreement with the heat flux contour plot of the ice/water exterior surface shown in Fig. 5(b). In regions where water evaporation is taking place, the surface heat flux is much higher than in other areas, where the heat transfer is of the form of natural convection (Eq. (4)) when at still air, or of the form forced convection (Eq. (6)) in the presence of wind. These plots show only half of the windshield, per the symmetry assumption, when viewed from the cabin inside along a direction normal to the windshield.

Figure 6 presents the time evolution of the liquid fraction,  $\gamma$ , at the surface of ice-water layer for a simulation with wind speed of 10 m/s and relative humidity of 100%. The time evolution of the liquid fraction is also an accurate representation of the development and spreading of the melting pattern on the windshield. Although not shown in the figure, initial breakthrough of the ice-layer occurs around 10 min. Subsequent gradual spreading of the melting region with time is clearly visible. At 40 min, 83% of the windshield is free from ice. At the same wind speed, when the relative humidity is 30% the ice-melting pattern development is shown in Fig. 7. Comparison between the two simulations indicates an apparent delay in melting when the humidity is 30%. The delay in melting is not evident early in the test ( $t < 1500$  s), as it takes some time for a pool of water to form on the windshield. The water evaporation rate increases with a rise in water temperature, leading to a delay in melting which is pronounced at later times.

At 40 min, evaporation takes enough heat from the ice-water layer so that the liquid fraction apparently falls below 1.0 at the surface or "re-freezing" starts to occur. This condition is seen in Fig. 7(f), which shows that re-freezing happens at the edge of the already formed water pool. This observation is indeed consistent as the heat source is supplied at the center of the pool.

Figure 8 shows percentage area melt of the windshield for three wind speeds considered in the study. Percentage area melt is defined as the ratio of the ice melted area to the area of the windshield. In still air, the humidity does not have a significant impact on the ice clearing rate (Fig. 8(a)). There is no appreciable difference among the four curves representing humidity levels of  $\phi = 20\%$ , 30%, 40% and

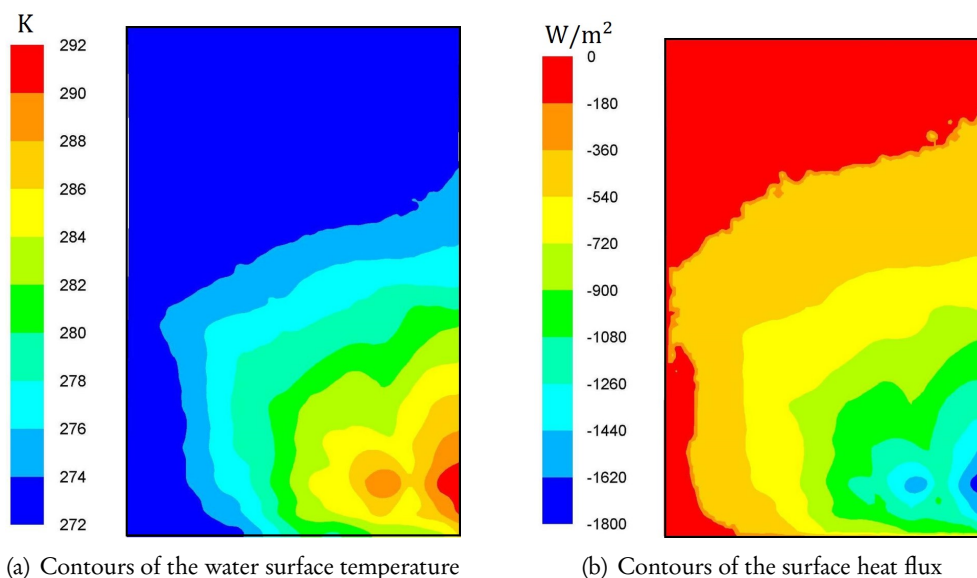


Fig. 5. Contours of the surface temperature and the surface heat flux of the ice-water layer at 2400 s. The wind speed is 10 m/s and the relative humidity is 30%.

100%. As the wind speed increases a clear departure from this behavior is evident from Figs. 8(b) and 8(c). At the wind speed of 10 m/s, low humidity levels significantly retard the ice clearing rate. Thus, there is gradual degradation of the ice-clearing performance as the relative humidity of the air increases.

Figure 8(c) indicates that the humidity does not affect the melting rates until about 1500 s. This is because it requires a certain amount of area of water surface exposure for enough evaporation to take place before sufficient heat energy is taken away from the ice-water layer. The increase in water temperature also helps the evaporation as evident from Eq. (2) and Fig. 1. Once these two contributions come into effect, a clear change in melting rates is evident. When the humidity is as low as 20% the melting rate slows down drastically, and the percentage area of the ice-melting seems to come to a limit.

Figure 9 shows time variation of cumulative mass of water evaporation during simulations. In still air (Fig. 9(a)) the evaporation rate is low, and less dependent on the humidity level. Figure 9(a) also shows that the water evaporation increases with the decrease in humidity level, as consistent with Eq. (2). An increase in rate of evaporation can be seen at a wind speed of 7.5 m/s. However, comparison of Figs. 9(b) and 9(c), shows that water evaporation has not increased much going from a wind speed of 7.5 m/s to 10 m/s. The reason for this behavior can be explained in conjunction with Fig. 8 which describes the ice-melting area. The tendency to increase the evaporative mass at a wind speed of 10 m/s is hindered by the fact that the water surface area exposed for evaporation is smaller compared to that at 7.5 m/s. It is also illustrative to look at the change in evaporative mass due to change in wind speed at a given humidity level. At the relative humidity of  $\phi = 100\%$ , there is no significant difference in the melting area at wind speeds of 7.5 m/s and 10 m/s (Figs. 8(b) and 8(c)), hence only a slight increase in water evaporation that is solely due to the change in wind speed can be seen.

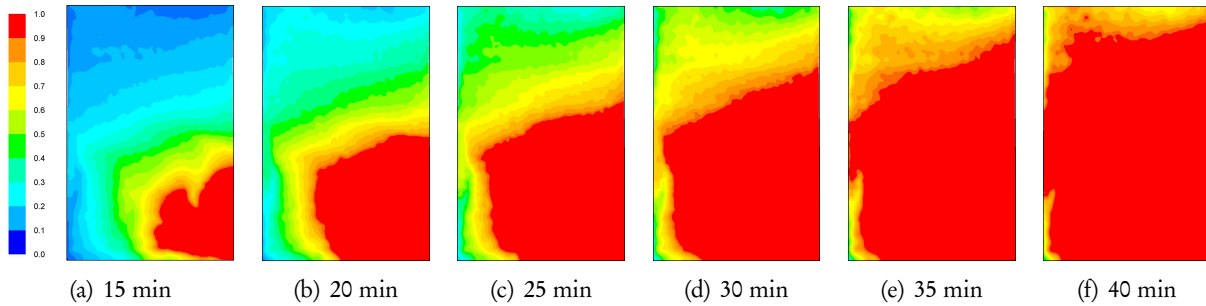


Fig. 6. Contours of liquid fraction  $\gamma$  of the ice layer: the wind speed is 10 m/s and the relative humidity is 100%.

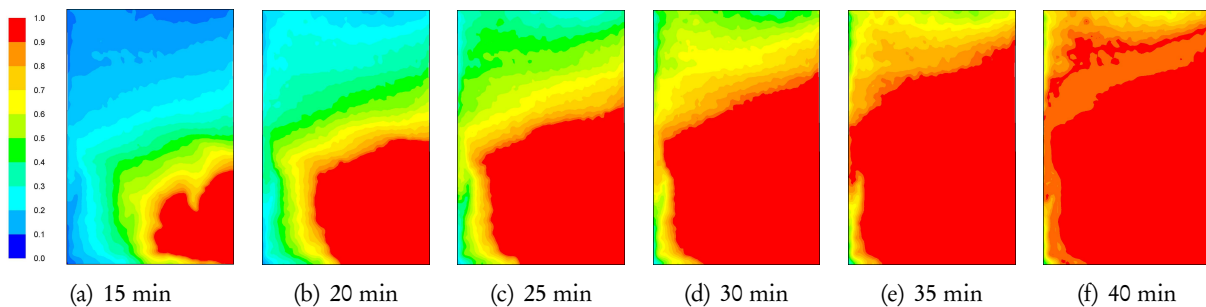


Fig. 7. Contours of liquid fraction  $\gamma$  of the ice layer: the wind speed is 10 m/s and the relative humidity is 30%.

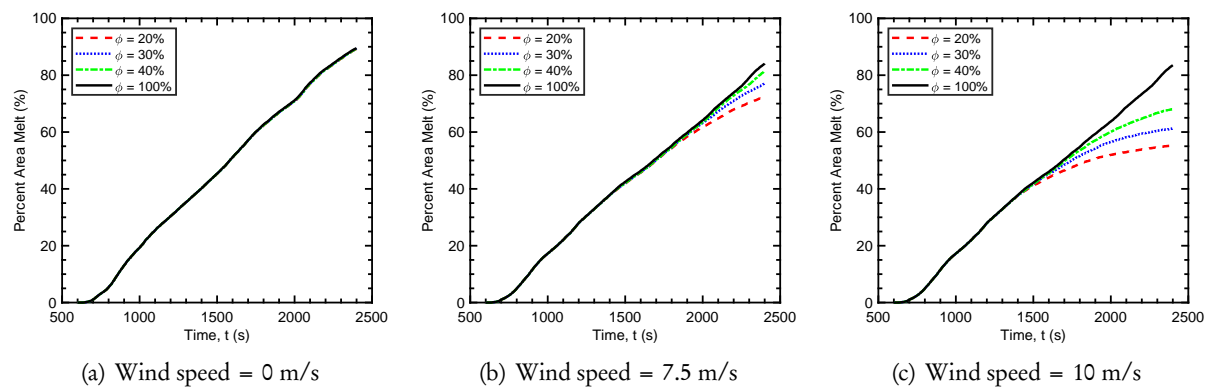


Fig. 8. The time evolution of the percentage area of ice-melt at different wind speeds.

#### 4. Discussion

It is worthwhile to compare the energy taken away by water evaporation to the energy associated with sensible heating and the energy used for melting ice. Referring to the data presented in Fig.5(a), at a surface water temperature of 290 K and at a wind speed of 10 m/s, the water evaporation rate is 0.6 g/m<sup>2</sup>s per Eq. (2). The latent heat associated with the evaporation is 1.47 kW/m<sup>2</sup>. With approximately a 0.44 m<sup>2</sup> area of exposed water, the heat loss due to evaporation is about 0.64 kW. The temperature of the warm air coming in to the cabin at the condition depicted in Fig. 7(f) is 327 K and the average cabin interior temperature is 285 K. Thus, the heat added to the cabin is approximately 1.27 kW, indicating that about 50% of incoming heat from the warm air is taken away by evaporation. In the absence of

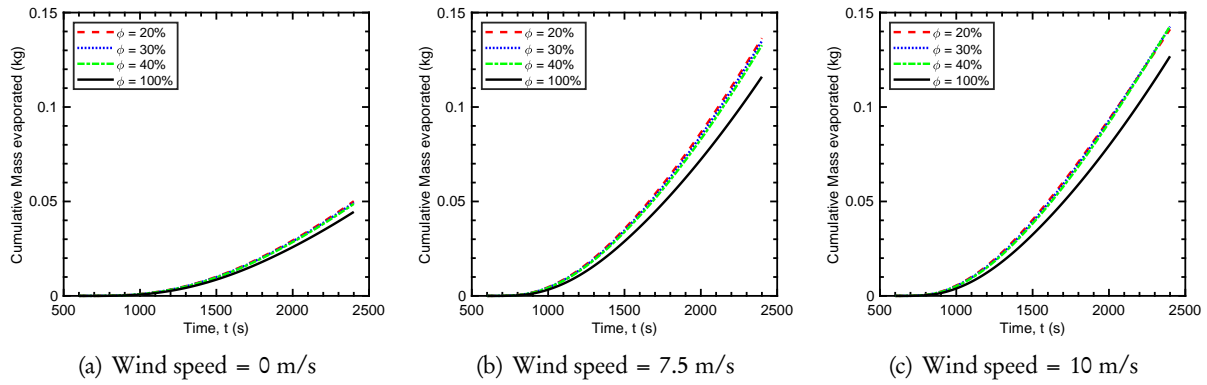


Fig. 9. The time evolution of cumulative mass evaporated at different wind speeds.

evaporation this heat is available for either sensible heat gain or for ice-melting. Some heat is taken away by the HVAC air that is discharged at the cabin temperature to the ambient. As this simple calculation illustrates, when the conditions are conducive, water evaporation can play a significant role in delaying ice melting.

In order to guarantee vehicle safety, mandatory requirements are set on ice-melting capability of the vehicle HVAC system. The ambient air humidity combined with the wind speed certainly affect the ice-clearing rate. As Fig. 10 indicates, at or near saturated air, the defrosting process is not much affected by the wind speed on the other hand, at low humidity levels a clear degradation is evident. This phenomenon can influence climatic wind tunnel tests, as well as the safety of a driver on the road in wintry conditions. During climatic wind tunnel tests, the humidity of the air and the wind speed are controllable parameters, whereas, they are nature dependent in the latter case.

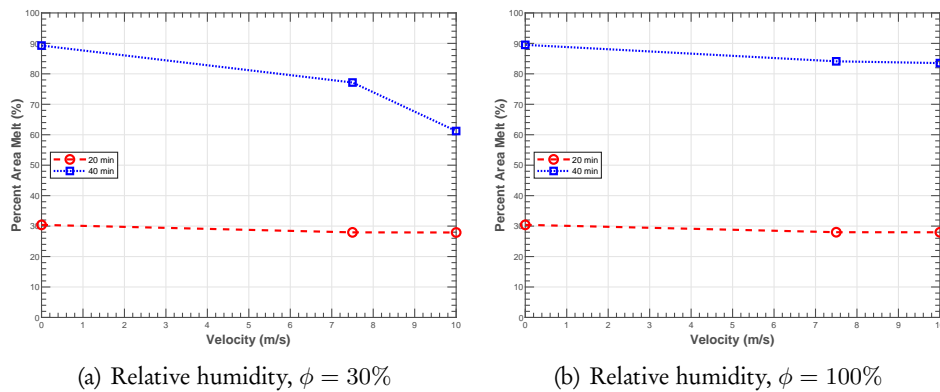


Fig. 10. The variation of percentage of ice melting area at 20 and 40 minutes with the wind speed. (a) Relative humidity,  $\phi = 30\%$ , and (b) Relative humidity,  $\phi = 100\%$ .

Figure 7(f) shows that at  $t = 2400$  s, some indication of re-freezing is taking place. Re-freezing can occur when the temperature of the water surface temperature is at the saturated liquid temperature and the heat conduction across the water film is less than the heat loss from the exposed surface due to water evaporation. In an idealized, one-dimensional case the condition for re-freezing to occur may be written as,

$$k_w \left[ \frac{\partial T}{\partial x} \right]_o < m_e h_{fg} \tag{8}$$

where,  $k_w$  is the thermal conductivity of water,  $x$  is the coordinate normal to the windshield and subscript  $o$  refers to the conditions at the outer surface of the ice-water layer.

The present study suggests (Fig. 8(c)) that percentage clearing may seem to reach about 68%, at a wind speed of 10 m/s and a relative humidity of 40%. Figure 11 shows this simulation continued until 4800 s in order to understand the behavior of the ice-water mixture over a longer period of time.

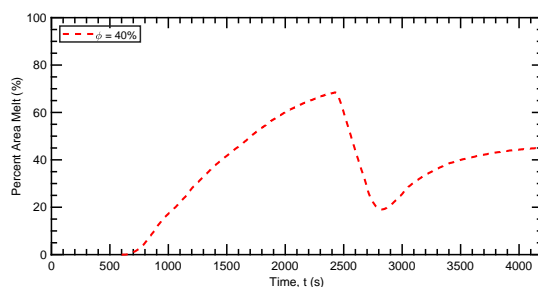


Fig. 11. Time evolution of the percentage ice melting area for a simulation extended up to 4200 s. Ambient air conditions: Relative humidity,  $\phi = 40\%$ , and wind speed = 10 m/s.

It should also be noted that, in the present study, the CFD model does not explicitly remove evaporated water from the computational domain. It is difficult to incorporate such phenomena involving vapor phase in a 3D full-scale vehicle level model. Such simulations require further studies, hence the deductions with regard to the re-freezing presented in this study are only cursory. The main purpose of the present article is to show that the air humidity and the wind speed can play a role in delaying the windshield defrosting due to water evaporation, and thereby directly affecting driver safety.

## 5. Conclusions

3D, full-scale, vehicle level CFD simulations are carried out to study the effect of water evaporation during an automotive windshield defrosting process. To that end, the ambient air humidity and the wind speed were used as the independent variables. The time it takes for the HVAC system to clear an ice-layer applied on the windshield glass exterior is considered as the measure of the vehicle defrosting performance.

When surrounding air humidity is low and the wind speed is high, ice-turned-water can evaporate off of the windshield outer surface. The evaporation takes heat away from the ice-melting process thereby delaying the ice-melting, and also reducing the defrosting performance. At high humidity levels the evaporation is low, and thus the defrosting performance is not much affected. However, when the wind speed is high, the humidity plays a significant role in retarding the speed of ice melting. When the ambient air is near saturation, the effect of humidity is less significant. Comparison of simulations conducted at wind speeds between 0 m/s and 10 m/s shows a significant difference in ice-melted area.

A note on how the range of parameters considered in the study relate to nature is in order. In general, at or near freezing temperatures, air holds a little moisture. There are recorded weather data that show the occurrence of sub-zero temperatures and low humidity conditions, simultaneously [32]. Some examples are, in Marion, Illinois on January 6-9, 2017 the temperatures were in the range ( $-7^{\circ}\text{C}$  -  $0^{\circ}\text{C}$ ) and the relative humidity levels were 40%–45%, and in Atlantic, Iowa on January 13-14, 2017 where the temperatures were in the range ( $-8^{\circ}\text{C}$  -  $-2^{\circ}\text{C}$ ) and the humidity levels were 30%–31%.

The simulations do not model removal of water evaporated from the ice-layer, but the effect is only modeled as a heat loss. Further work is necessary to include such complexities into the simulations.

## Acknowledgements

The authors gratefully acknowledge the financial support by the Engineering Faculty Research Fund, Faculty of Engineering, Chulalongkorn University (Contract No. 001/2560). Authors would like to thank BETA-CAE Systems for providing ANSA software for building the CFD model. Thanks are also

due to Kwanchai Chinwicharnam and Pawarit Laosunthara for their assistance in writing C-code, and to Dr. Joshua Staubs for editorial comments.

## References

- [1] SAE, “J902A: Passenger Car Windshield Defrosting Systems,” *SAE Publications*, pp. 976–978, 1967.
- [2] B. S. AbdulNour, “Numerical simulation of vehicle defroster flow field,” SAE Technical Paper, Tech. Rep., 1998.
- [3] A. Aroussi and A. Hassan, “Vehicle side-window defrosting and demisting process,” in *EACC 2003 1st European Automotive CFD Conference, Bingen, Germany 25-26 June 2003*, 2003, pp. 155–163.
- [4] A. Aroussi, A. Hassan, and Y. Morsi, “Numerical simulation of the airflow over and heat transfer through a vehicle windshield defrosting and demisting system,” *Heat and Mass Transfer*, vol. 39, no. 5-6, pp. 401–405, 2003.
- [5] R. A. Brewster, S. Frik, and F. Werner, “Computational analysis of automotive windshield de-icing with comparison to test data,” SAE Technical Paper, Tech. Rep. 971833, 1997.
- [6] A. Farag and L.-J. Huang, “Cfd analysis and validation of automotive windshield de-icing simulation,” SAE Technical Paper, Tech. Rep., 2003.
- [7] J.-G. Lee, Y. Jiang, A. Przekwas, and M. Sioshansi, “Validation of computational vehicle windshield de-icing process,” SAE Technical Paper, Tech. Rep., 1994.
- [8] S. Roy, H. Kumar, and R. Anderson, “Efficient defrosting of an inclined flat surface,” *International Journal of Heat and Mass Transfer*, vol. 48, no. 13, pp. 2613–2624, 2005.
- [9] W. Park, M. Park, Y. Jung, and K. Jang, “Numerical study of defrosting phenomena of automotive windshield glass,” *Numerical Heat Transfer, Part A: Applications*, vol. 47, no. 7, pp. 725–739, 2005.
- [10] M. Kader, Y. Youn, Y. Jun, and K. Lee, “Characterization of the hvac performance with defroster grillers and instrument panel registers,” *International Journal of Automotive Technology*, vol. 10, no. 3, pp. 305–312, 2009.
- [11] W. Yang, W. Shi, F. Guo, and W. Yang, “Flow field simulation and performance analysis of hvac defrosting duct,” in *2nd International Conference on Electronic & Mechanical Engineering and Information Technology (EMEIT-2012), China*, 2012, pp. 297–300.
- [12] S. Kang, M. Kader, Y. Jun, and K. Lee, “Automobile defrosting system analysis through a full-scale model,” *International Journal of Automotive Technology*, vol. 12, no. 1, pp. 39–44, 2011.
- [13] N. Kandasamy and S. Whelan, “Sensitivity analysis of windshield defrost characteristics impact on occupant thermal comfort,” SAE Technical Paper, Tech. Rep., 2017.
- [14] M. Shojaeefard, G. Molaeimanesh, N. Aghamirzaei, S. Ghezelbiglo, and B. Zeinolabedini, “Numerical evaluation of the defrosting/defogging performance of hvac system in the main product of the national vehicle platform,” *International Journal of Automotive Engineering*, vol. 5, no. 4, pp. 2006–2016, 2015.
- [15] M. Nemes, M. Martinchick, and S. Ibri, “Cabin heating and windshield defrosting for extended range electric, pure electric, & plug-in hybrid vehicles,” *SAE International Journal of Alternative Powertrains*, vol. 1, no. 1, pp. 12–18, 2012.
- [16] R. Tang and Y. Etzion, “Comparative studies on the water evaporation rate from a wetted surface and that from a free water surface,” *Building and Environment*, vol. 39, no. 1, pp. 77–86, 2004.
- [17] F. Asdrubali, “A scale model to evaluate water evaporation from indoor swimming pools,” *Energy and Buildings*, vol. 41, no. 3, pp. 311–319, 2009.
- [18] M. M. Shah, “Improved method for calculating evaporation from indoor water pools,” *Energy and Buildings*, vol. 49, pp. 306–309, 2012.
- [19] —, “Methods for calculation of evaporation from swimming pools and other water surfaces,” *ASHRAE Transactions*, vol. 120, no. 2, pp. 3–17, 2014.
- [20] T. Lu, X. Lü, and M. Viljanen, “Prediction of water evaporation rate for indoor swimming hall using neural networks,” *Energy and Buildings*, vol. 81, pp. 268–280, 2014.

- [21] ASHRAE, "Hvac applications," *ASHRAE Handbook, Fundamentals*, 2007.
- [22] E. Sartori, "A critical review on equations employed for the calculation of the evaporation rate from free water surfaces," *Solar energy*, vol. 68, no. 1, pp. 77–89, 2000.
- [23] M. Örvös, V. Szabó, and T. Poós, "Rate of evaporation from the free surface of a heated liquid," *Journal of Applied Mechanics and Technical Physics*, vol. 57, no. 6, pp. 1108–1117, 2016.
- [24] J. L. F. Blázquez, I. R. Maestre, F. J. G. Gallero, and P. Á. Gómez, "A new practical cfd-based methodology to calculate the evaporation rate in indoor swimming pools," *Energy and Buildings*, vol. 149, pp. 133–141, 2017.
- [25] C. C. Smith, G. Löf, and R. Jones, "Measurement and analysis of evaporation from an inactive outdoor swimming pool," *Solar Energy*, vol. 53, no. 1, pp. 3–8, 1994.
- [26] A. Jodat, M. Moghiman, and M. Anbarsooz, "Experimental comparison of the ability of dalton based and similarity theory correlations to predict water evaporation rate in different convection regimes," *Heat and Mass Transfer*, vol. 48, no. 8, pp. 1397–1406, 2012.
- [27] A. M. Raimundo, A. R. Gaspar, A. V. M. Oliveira, and D. A. Quintela, "Wind tunnel measurements and numerical simulations of water evaporation in forced convection airflow," *International Journal of Thermal Sciences*, vol. 86, pp. 28–40, 2014.
- [28] P. J. Flatau, R. L. Walko, and W. R. Cotton, "Polynomial fits to saturation vapor pressure," *Journal of Applied Meteorology*, vol. 31, no. 12, pp. 1507–1513, 1992.
- [29] A. Malatip, N. Wansophark, and P. Dechaumphai, "Finite element method for analysis of conjugate heat transfer between solid and unsteady viscous flow," *Engineering Journal*, vol. 13, no. 2, pp. 43–58, 2009.
- [30] C. Suvanjumrat, "Implementation and validation of openfoam for thermal convection of airflow," *Engineering Journal*, vol. 21, no. 5, pp. 225–241, 2017.
- [31] T. L. Bergman, F. P. Incropera, D. P. DeWitt, and A. S. Lavine, *Fundamentals of Heat and Mass Transfer*. John Wiley & Sons, 2011.
- [32] "Weather underground," <https://www.wunderground.com/>, accessed: 2018.